

# I/Q IMBALANCE COMPENSATION ALGORITHM BASED ON NEURAL NETWORKS

Botond Sandor Kirei, Marina Topa, Marius Neag, Raul Ciprian Onet

## Abstract:

*This paper proposed an I/Q imbalance compensation algorithm based on neural networks, suitable for low-IF receivers. First, the low-IF receiver architecture and the phenomena of I/Q imbalance (also referred as image interference) are described. The standard solution - using a complex LMS adaptive filter, which separates the desired, and image signals - is limited in that the recovered signal remains affected by the I/Q imbalance; the filter proposed here corrects this drawback. The functionality, convergence and stability of the neural network based filter are demonstrated through extensive computer simulations. A sizing example is also given - deduction of the number of sample necessary in order to achieve a -60 dB image rejection - along with the time domain behaviour of the resulting neural network.*

**Keywords:** low-IF receiver, I/Q imbalance compensation, image rejection, and neural networks.

## 1. Introduction

In the last two decades, increased consumer interest in wireless communication devices has resulted in significant technical developments. Nowadays rigorous efforts are invested in development of multistandard receivers with low cost, single chip implementation, low power consumption, etc. The main contenders for title of most popular architecture for integrated receivers in this century have been so far the zero-IF and low-IF receivers. Both architectures are suitable for integration and have been used to develop complex SoC, combining analog front-ends and digital base-band signal processing on a single chip. However, each of these architectures has serious drawbacks, such as: for the low-IF receiver, non-idealities inherent to physical implementations result in amplitude and phase mismatches between the I and Q signal paths; thus the desired signal is degraded by interferences ("leakage") from the adjacent band signal, making it mandatory to use image rejection filters. The desired signal in zero-IF receiver is degraded by time variant (low-frequency) DC offsets caused by self-mixing and leakages between the local oscillator and the RF path; such errors are very difficult to eliminate or compensate for.

Numerous image rejection algorithms and filters for low-IF receivers are described in the literature. An interesting solid state circuit solution has been recently proposed in [1]: an adaptive filter based on the sign detection LMS algorithm that allows for a simple hardware implementation at the cost of lower estimation accuracy.

Depending on the quantization noise, it can achieve an image to signal ratio (ISR) of approximately 60dB. Reference [2] presents a non-data-aided image rejection algorithm. Exploring the mutual independence property of the desired and image signals the measure of the interference can be determined and the initial signals restored. By using the simulation model presented in [2], one can see that the desired signal expression comprises a scaling factor that is phase mismatch dependent, thus making the filter vulnerable to phase errors. A similar problem limits the solution proposed in [3]: there a modified complex LMS filter is used in order to reject the image frequencies; the amplitude errors are corrected but the phase errors are not fully cancelled. Reference [4] shows how a small phase mismatch can reduce the ISR achieved by an LMS filter down to 30 dB. Other solutions are based on blind source (or signal) separation [5].

The earliest implementations make use of a calibration tone signal applied at the front-end of the low-IF receiver [6]. These solutions are becoming obsolete, as they required additional calibration time and hardware for the tone generation.

The image rejection filter proposed here is based on the one described in [3]. As mentioned above, the major drawback of this implementation is its relatively large sensitivity to phase errors and mismatches between I and Q signal paths, highlighted by the presence of a phase mismatch dependent in the expression of the resulting wanted signal. The solution presented here aims at correcting this problem by using neural networks to implement the LMS adapting function, thus eliminating the scaling factor. Note that although there are several noise sources in a low-IF receivers (noise introduced by the analog mixer, quantization noise due to the analog-digital conversion, image interference, etc.), this paper analyses only the effect of image interference.

In Section 2 and 3 the low-IF receiver architecture and the image interference - also referred as I/Q imbalance - are briefly presented. Section 4 describes the enhanced image rejection filter based on a neural network. For a better understanding, the combination of two neurons resulting in the filter studied in [3] and [4] is first presented. Then the newly proposed combination of four neurons, that realizes the enhanced image rejection, is described. Section 5 contains simulation results obtained in Simulink; last but not least, conclusions are drawn in Section 6.

## 2. The low-IF receiver architecture

Fig. 1 presents the generic low-IF receiver architecture. The radio frequency (RF) signal captured by the

antenna is filtered by the band-select filter BPF and amplified by the low-noise amplifier LNA. Image cancellation can be achieved at this point, but requires narrow band filtering and thus increases significantly the complexity and cost of the device. The RF signal is down converted to an intermediary frequency (IF) by using a quadrature local-oscillator signal  $x_{LO}$ ; this way a complex low-IF signal is generated, which can be represented by in-phase and quadrature signals, usually named  $I$  and  $Q$  ( $I(t)$  and  $Q(t)$ ). The IF signals are low-pass filtered by the LPFs then sampled by the ADCs, resulting in the  $I(n)$  and  $Q(n)$  strings. The base band demodulation and image rejection are done in the digital domain. It should be noted that some implementations - not discussed in this paper - use image-rejecting complex LPFs.

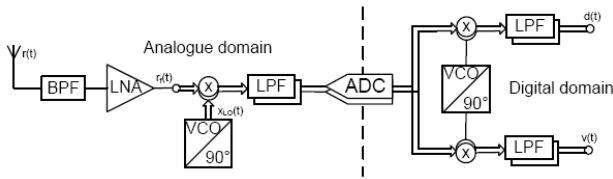


Fig. 1. The low-IF receiver architecture.

Let us consider that the RF signal  $r(t)$  at the input of the receiver is given by:

$$r(t) = z(t) \cdot e^{+j2\pi f_c t} + z^*(t) \cdot e^{-j2\pi f_c t} \quad (1)$$

where the carried signal  $z(t)$  is a combination of the desired signal  $s(t)$  and the interferer  $i(t)$  from the adjacent band:

$$z(t) = s(t) \cdot e^{+j2\pi f_i t} + i(t) \cdot e^{-j2\pi f_i t} \quad (2)$$

The filtered intermediary frequency signal is sampled by the ADC resulting in:

$$r_{IF}(n) = s(n) \cdot e^{j2\pi f_i nT} + i(n) \cdot e^{-j2\pi f_i nT} \quad (3)$$

The low-IF receiver will produce two output signals. The first one,  $d(n)$ , is the intermediary frequency signal demodulated on the cosine carrier and filtered. The second signal,  $v(n)$ , results from the intermediary frequency signal by demodulation with the sine carrier. Their expressions are:

$$d(n) = \frac{1}{2} [s(n) + i(n)] \quad (4)$$

$$v(n) = \frac{1}{2} [s(n) - i(n)]$$

### 3. I/Q imbalance in low-IF receivers

In a real-life implementation the local oscillator signal,  $x_{LO}$ , is affected by amplitude and phase errors than can be expressed by:

$$x_{LO}(t) = \cos(2\pi f_{LO}t) - j \cdot g \cdot \sin(2\pi f_{LO}t + \phi) \quad (5)$$

where  $g$  is the amplitude and  $\phi$  the phase errors. These errors have a slow variation in time, so during the signal processing they can be considered constant. At down-

conversion these errors will cause interferences between the I/Q paths; phase and amplitude mismatches between the I/Q signal paths (LPF and ADCs) are additional causes of such interferences. This effect is usually called I/Q imbalance. In order to simplify the mathematical expressions one can introduce the *I/Q imbalance* parameters, defined as follows:

$$k_1 = \frac{1+g \cdot e^{-j\phi}}{2}; k_2 = \frac{1-g \cdot e^{+j\phi}}{2} \quad (6)$$

The IF signal can now be expressed using the I/Q imbalance parameters:

$$I(t) + jQ(t) = LPF\{r(t) \cdot x_{LO}\} = k_1 \cdot z(t) + k_2 \cdot z^*(t) \quad (7)$$

where LPF stands for the low-pass filtering function. The IF signal spectrum is depicted in Fig. 2b. After the ADC sampling and conversion, the digitised IF signal is down-converted into the base band, yielding the following complex signals:

$$\begin{aligned} d(n) &= d_r(n) + jd_i(n) = LPF\{I(n) \cdot e^{-j2\pi f_{IF}nT}\} = \\ &= k_1 \cdot s(n) + k_2 \cdot i^*(n) \\ v(n) &= v_r(n) + jv_i(n) = LPF\{Q(n) \cdot e^{+j2\pi f_{IF}nT}\} = \\ &= k_1 \cdot i(n) + k_2 \cdot s^*(n) \end{aligned} \quad (8)$$

Note that  $s(n)$  and  $i(n)$  are complex signals, as well.

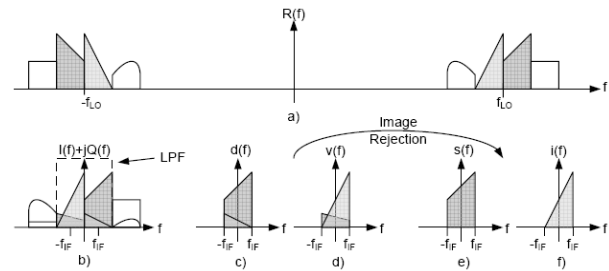


Fig. 2. a) Spectrum of the RF signal. b) Spectrum of IF signal. c) Spectrum of the mixture signal  $d(n)$ . d) Spectrum of the mixture signal  $v(n)$ . e) Spectrum of desired signal  $s(n)$ . f) Spectrum of interferer signal  $i(n)$ .

The signal  $d(n)$ , depicted in Fig. 2c, contains the desired signal  $s(n)$  (spectrum shown in Fig. 2e and the conjugate of the interferer  $i^*(n)$ ). Likewise  $v(n)$ , depicted in Fig. 2d, contains the interferer signal  $i(n)$  (spectrum shown in Fig. 2f) and the conjugate of the desired signal  $s^*(n)$ . Therefore they are called "mixture" signals.

The equations (6) can be written in compact matrix form as follows:

$$\begin{bmatrix} d(n) \\ v^*(n) \end{bmatrix} = \begin{bmatrix} k_1 & k_2 \\ k_{21}^* & k^* \end{bmatrix} \cdot \begin{bmatrix} s(n) \\ i^*(n) \end{bmatrix} \quad (9)$$

### 4. Image rejection filter

The signal flow chart in Fig. 3 corresponds to the operation of a standard LMS image rejection filter, such as the one proposed in [3]; it has two outputs, one for the desired and one for the interfering signal. In this case the neurons are not performing an LMS adaptation but an adaptive prediction operation. Thus one can write two

cost functions to force the outputs to represent the desired and interfered signals:

$$\begin{aligned} \xi_1 &= E \left\{ \left| r_1(n) - w_1^* \cdot x_1(n) \right|^2 \right\} \\ \xi_2 &= E \left\{ \left| r_2(n) - w_2^* \cdot x_2(n) \right|^2 \right\} \end{aligned} \quad (10)$$

By substituting in equation (8) the desired signals  $r_1(n)$  and  $r_2(n)$  with the corresponding values of  $d(n)$  and  $v^*(n)$  and the pair of input signal  $x_1(n)$  and  $x_2(n)$  with  $v^*(n)$  and  $d(n)$  it results:

$$\begin{aligned} \xi_1 &= E \left\{ \left| d(n) - w_1^* \cdot v^*(n) \right|^2 \right\} \rightarrow i^*(n) \\ \xi_2 &= E \left\{ \left| v^*(n) - w_1^* \cdot d(n) \right|^2 \right\} \rightarrow s(n) \end{aligned} \quad (11)$$

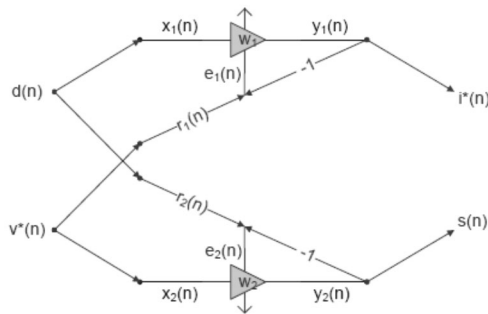


Fig. 3. Signal flow graph of image rejection filter.

For implementing a recursive process similar to LMS weight adaptation several considerations have to be made: 1. One pair of adapting neurons implies the usage of two weight values. 2. Because the neuron performs a prediction operation, the input signal  $x_1(n)$  and  $x_2(n)$  should be replaced by the errors  $e_2(n)$ , respectively  $e_1(n)$ , representing the values that are rejected. The resulting recursive process for the neurons coefficients is described by the following expressions:

$$\begin{cases} w_1(n+1) = w_1(n) + 2 \cdot \mu_1 \cdot e_1^*(n) \cdot e_2(n) \\ w_2(n+1) = w_2(n) + 2 \cdot \mu_2 \cdot e_2^*(n) \cdot e_1(n) \end{cases} \quad (12)$$

When  $w_1$  and  $w_2$  are adapted the following conditions are fulfilled:

$$\begin{cases} k_2 = w_1^*(n) \cdot k_1^* \\ k_1^* = w_2^*(n) \cdot k_2 \end{cases} \quad (13)$$

For the predicted signals the corresponding expressions are:

$$\begin{aligned} y_1(n) &= (k_2 - w_2^*(n) \cdot k_1^*) \cdot i^*(n) \\ y_2(n) &= (k_2^* - w_1^*(n) \cdot k_1) \cdot s(n) \end{aligned} \quad (14)$$

The imbalance parameters  $k_1$  and  $k_2$  still contain the phase error introduced in the mixing stage, but the signals are successfully separated. Equation (14) is equivalent to the result obtained in [3].

Fig. 4 presents the enhanced image rejection filters flow chart: one can observe that the filter contains four neurons, thus four cost functions will be processed. Two neurons are following the rules represented by equation

(15) while the complementary neurons aim to adapt in order to reach the following objective:

$$\begin{aligned} \xi_{11} &= E \left\{ \left| d(n) - w_{11}^* \cdot v^*(n) \right|^2 \right\} \rightarrow i^*(n) \\ \xi_{12} &= E \left\{ \left| v^*(n) - w_{12}^* \cdot d(n) \right|^2 \right\} \rightarrow s(n) \\ \xi_{21} &= E \left\{ \left| d(n) - w_{21} \cdot v^*(n) \right|^2 \right\} \rightarrow s(n) \\ \xi_{22} &= E \left\{ \left| v^*(n) - w_{22} \cdot d(n) \right|^2 \right\} \rightarrow i^*(n) \end{aligned} \quad (15)$$

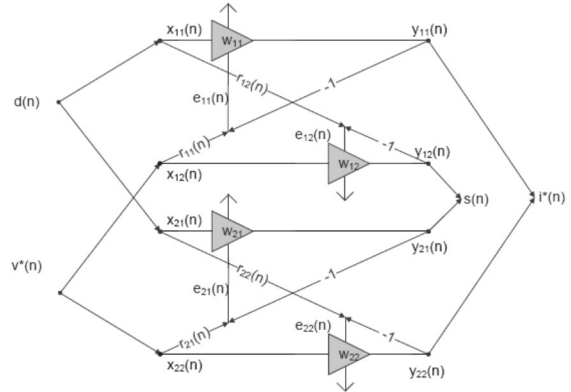


Fig. 4. Signal flow graph of proposed filter.

Based on same considerations, the neuron coefficients for the recursive processes result:

$$\begin{cases} w_{11}(n+1) = w_{11}(n) + 2 \cdot \mu_{11} \cdot e_{12}(n) \cdot e_{11}^*(n) \\ w_{12}(n+1) = w_{12}(n) + 2 \cdot \mu_{12} \cdot e_{11}(n) \cdot e_{12}^*(n) \\ w_{21}(n+1) = w_{21}(n) - 2 \cdot \mu_{21} \cdot e_{21}(n) \cdot e_{22}^*(n) \\ w_{22}(n+1) = w_{22}(n) - 2 \cdot \mu_{22} \cdot e_{22}(n) \cdot e_{21}^*(n) \end{cases} \quad (16)$$

Similarly, for the predicted signals one obtains the expressions:

$$\begin{aligned} y_{11}(n) &= (k_2 - w_{12}^*(n) \cdot k_1^*) \cdot i^*(n); y_{12}(n) = (k_2^* - w_{11}^*(n) \cdot k_1) \cdot s(n) \\ y_{21}(n) &= (k_1 - w_{22}(n) \cdot k_2^*) \cdot s(n); y_{22}(n) = (k_1^* - w_{21}(n) \cdot k_2) \cdot i^*(n) \end{aligned} \quad (17)$$

From this point on the recovery of the desired signal consists in a gain correction given by the weight values; since  $k_1 + k_2^* = k_2 + k_1^* = 1$  it results:

$$\begin{aligned} \frac{y_{11}(n)}{1 - w_{12}^*(n) \cdot w_{11}^*(n)} + \frac{y_{22}(n)}{1 - w_{21}(n) \cdot w_{22}(n)} &= (k_2 + k_1^*) \cdot i^*(n) = i^*(n) \\ \frac{y_{12}(n)}{1 - w_{11}^*(n) \cdot w_{12}^*(n)} + \frac{y_{21}(n)}{(1 - w_{22}(n) \cdot w_{21}(n))} &= (k_1 + k_2^*) \cdot s(n) = s(n) \end{aligned} \quad (18)$$

### 5. Simulations

Since the presented image rejection filter is an adaptive one, stability, convergence and performance issues need to be carefully analysed. Extensive simulations have been run using Simulink models. In the example presented here the desired signal  $s(n)$  is an 8-QAM coded while the interferer (adjacent-channel)  $i(n)$  is 6-QAM. The  $d(n)$  and  $v(n)$  mixtures applied to the filter are obtained from the linear combination of  $s(n)$  and  $i(n)$  considering relative large values for the amplitude and phase errors:  $g=1.2$  and  $\varphi=10^\circ$  (see equations 6 and 9). Note that in

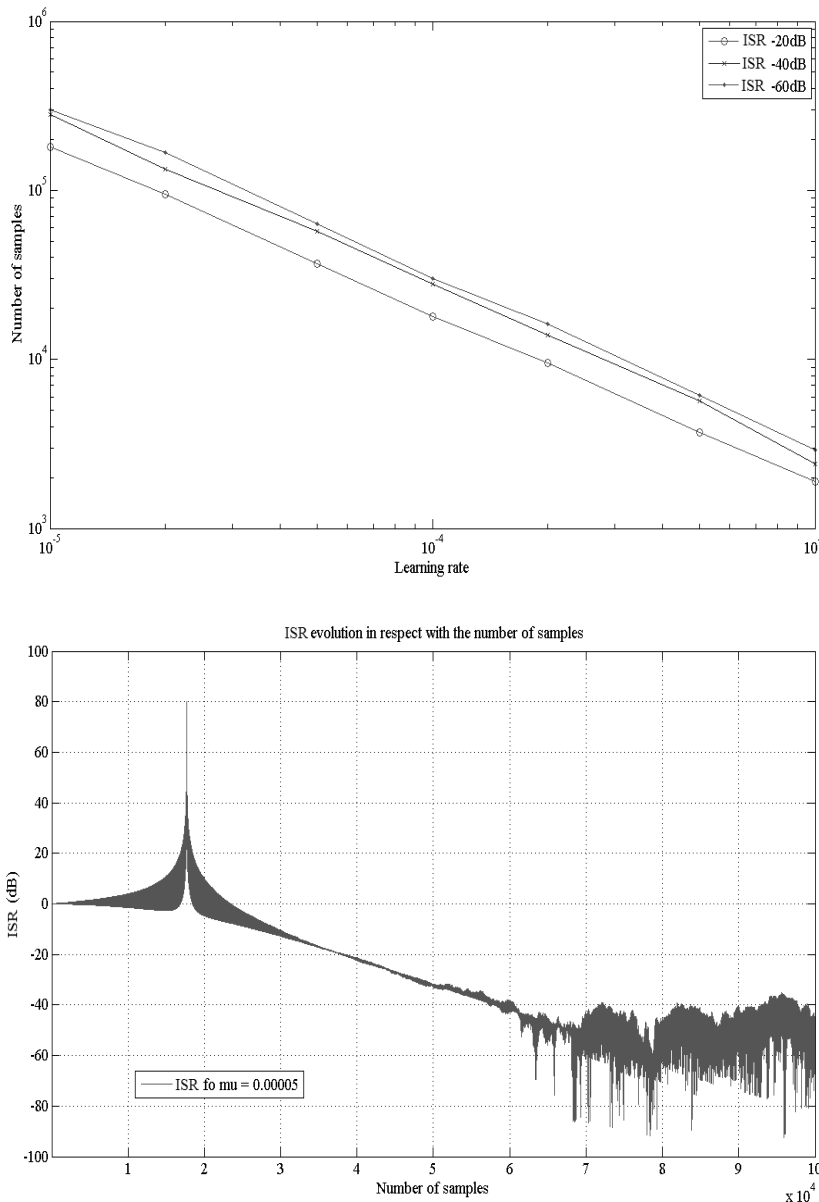


Fig. 5. a) Number of samples necessary to achieve a given ISR, as a function of the learning rate; b) ISR evolution in time for  $\mu=0.0005$ .

nowadays-integrated radios the amplitude mismatch between the I/Q branch is 1-2% and the phase mismatch is well below  $5^\circ$ .

Fig. 5a gives the number of samples necessary to reach a target ISR (-20, -40 and -60 dB) for different learning rates. From this graph an optimum value for the learning rate can be chosen, making a trade off between adaptation time and performance.

By analysing these plots one can conclude that by decreasing the learning rate, the time to reach a given ISR increases exponentially. On the other hand, by decreasing the learning rate a higher precision filtering is achieved.

The convergence of this system has not been proven mathematically but extensive simulations over a large range of conditions have shown that the filter always converges. Fig. 5b presents a typical example of such simulation: it shows the evolution of ISR from the first sample until the filter is adapted. The learning rate value

was set to  $\mu=0.0005$  based on previous simulation results. One can observe that at the beginning the filter is not stabilized, it does not reject the image signals, and the ISR values are meaningless; after about 18 K samples the adaptation begins and the ISR value is decreasing monotonously; after approximately 70 K samples the filter hits a resting point, and the ISR tends to vary between two values. This is because the weight values of the neurons can move around the optimal solution with the freedom given by the learning rate.

## 6. Conclusions

This paper proposed an I/Q imbalance compensation algorithm using neural networks, able to increase significantly the image rejection ratio of low-IF receivers. The new algorithm was based on an LMS filter solution proposed in the literature but solves a significant drawback of that filter, its sensibility to phase imbalances. This improvement was achieved by implementing an additional

adaptive loop using neural networks.

A Simulink model was developed and extensive simulations were run in order to demonstrate the effectiveness of the proposed algorithm and study its dynamic behaviour and convergence. They shown that the system converges over a wide range of conditions and it can provide ISRs better than 60 dB, even if the analog front-end introduces significant (larger than usual) amplitude and phase imbalances. There is a trade off between ISR and the learning rate/adaptation time.

Further developments consist of implementing the proposed filter on an FPGA. The FPGA integration will be helped by the fact that the Simulink model was created so that it can serve like an RTL description of the filter. Another direction is to speed up the learning process by the usage of variable learning rate or other similar methods.

### ACKNOWLEDGMENTS

This work was partly supported by the Romanian National University Research Council under Grant TD 428/2007 entitled Contributions to Designing and Implementing Integrated Poly-phase Filters for Wireless Applications.

### AUTHORS

**Botond Sandor Kirei\***, **Marina Topa**, **Marius Neag**, **Raul Ciprian Onet** - Technical University from Cluj-Napoca, Department of Basis of Electronics, C. Daicoviciu. 15, 400020 Cluj-Napoca, Romania. E-mails: {botond.kirei, marina.topa, irina.dornean}@bel.utcluj.ro.

\* Corresponding author

### References

- [1] Lerstaveesin S., Song B.-S., "A Complex Image Rejection Circuit with Sign Detection Only", *IEEE Journal on Solid-State Circuits*, vol. 41, no. 12, December 2006, pp. 2693-2702.
- [2] Gil Gye-Tae, Kim Young-Doo, Lee Yong H., "Non-Data-Aided Approach to I/Q Mismatch Compensation in Low-IF Receivers", *Transaction on Signal Processing*, vol. 55, no. 7, July 2007, pp. 3360-3365.
- [3] Yu L., Snelgrove W. M., "A Novel Adaptive Mismatch Cancellation System for Quadrature IF Radio Receivers", *IEEE Trans. on Circuits and Systems II: Analog and Digital Signal Processing*, vol. 46, no. 6, June 1999, pp. 789-801.
- [4] Kirei B. S., Dornean I., Topa M., "Image Rejection Filter Based on Complex LMS Filter for Low-IF Receiver". In: *Proceedings of IEEE - ELMAR 2008*, vol. 1, Zadar, Croatia, 10<sup>th</sup>-12<sup>th</sup> September 2008, ISBN 978-953-7044-08-4, pp. 203-206.
- [5] Windisch M., Fettweis G., "Blind I/Q Imbalance Parameter Estimation And Compensation In Low-IF Receivers". In: *IEEE Proceedings of 1<sup>st</sup> International Symposium on Control, Communications and Signal Processing (ISCCSP '04)*, Hammamet, Tunisia, March 2004.
- [6] Glas J.P.F., "Digital I/Q Imbalance Compensations in a Low-IF Receiver", *IEEE Global Telecommunications Conference 1998 (GLOBECOM'98). The Bridge to Global Integration*, vol. 3, 1998, pp. 1461-1466.
- [7] Kiss P., Arias J., Li D., Boccuzzi V., "Stable high-order

delta-sigma DACs". In: *IEEE Proceeding of the 2003 International Symposium on Circuits and Systems*, vol. 1, May 2003, pp. 985-988.

- [8] Farhang-Boroujeny B., *Adaptive Filters - Theory and Applications*, John Wiley & Sons, 1998, ISBN 0-471-98337-3, pp. 178-182.
- [9] Haykin S., *Neural Networks - A Comprehensive Foundation*, Prentice Hall, 1999, ISBN 0-7803-3494-9, pp. 118-137.